UNIVERSIDAD DE SONORA

DIVISIÓN DE CIENCIAS EXACTAS Y NATURALES
DEPARTAMENTO DE INVESTIGACIÓN EN FÍSICA

MEASUREMENTS OF THE LARGE HADRON COLLIDER LUMINOSITY USING THE CMS SILICON PIXEL DETECTOR

THESIS

in partial fulfillment of the requirements for the degree of:

Maestría en Ciencias (Física)

By:

Luis Enrique CUEVAS PICOS

Director:

Dr. Jose Feliciano BENITEZ RUBIO

Hermosillo, Sonora   May, 2023

Acknowledgements

Abstract

The calibration of the luminosity measurement from the analysis of the van der Meer scanning program for the CMS experiment in the 2022 proton-proton collision data-taking at $\sqrt{s} =$ 13.6 TeV with the CMS Silicon Pixel detector is described. The data collection period was on November 11 for the LHC fill 8381, the recorded data collected was reprocessed along with a selection of good modules based on luminosity stability studies. The Analysis of the van der Meer scans with some especific corrections present results in the calibration constant $\sigma_{vis} = 4163 \pm 3 (\text{stat.}) \pm 12 (\text{syst.})$ mb.

Resumen

Table of contents

List of figures

List of tables

Chapter 1

Introduction

Particle physics is the branch of physics that focuses on studying the fundamental particles and forces that make up matter and radiation in the universe. The Standard Model classifies the fundamental particles and their interactions as fermions, which are matter particles, and bosons, which are force-carrying particles. High-energy particle accelerators are used to study these interactions by measuring various parameters and properties of the particles produced during collisions.

This chapter provides a brief overview of elementary particles, particle colliders, and the measurement of their performance. It emphasizes the concepts and definitions necessary for understanding the thesis project.

1.1 Fundamental Particles

The universe is composed of several different particles. Atoms are bound states of negatively charged electrons (e^-), which orbit around a central nucleus consisting of positively charged protons (p) and electrically neutral neutrons (n). The electrons are bound to the nucleus by the electrostatic attraction between opposite charges, while the protons and neutrons are held together by the strong nuclear force. Completing the fundamental interactions of particle physics are the weak force and gravity. The weak force is responsible for nuclear -decays and nuclear fusion, while gravity, although extremely weak, is always attractive and therefore responsible for the large-scale structure in the universe. While this is a simple physical model, at higher energy scales, more complex structures are observed, leading to the discovery of 17 fundamental particles that make up our entire universe. These particles are divided into two groups: fermions with spin $1/2$ and bosons with integer spin [1].

Fermions are the particles that make constitute, consisting of twelve fundamental particles classified into two types: leptons and quarks. These particles are further divided into three generations, with each member of a higher generation having a greater mass than the corresponding particle of the previous generation. The six leptons include three charged particles: electron (e), muon (μ), and tau (τ), as well as their corresponding neutrinos: electron-neutrino (ν_e), muon-neutrino (ν_μ), and tau-neutrino (ν_τ). Quarks, on the other hand, can only be found in particles called hadrons. The group of quarks consists of the up quark (u), down quark (d), charm quark (c), strange quark (s), top quark (t), and bottom quark (b) [2]. The properties of these twelve particles are summarized in Table 1.1.

Table 1.1 The twelve fundamental fermions divided into quarks and leptons. The masses of the quarks are the current masses.

	Leptons				**Quarks**			
	Particle		Q	mass/GeV	Particle		Q	mass/GeV
First	electron	(e^-)	-1	0.0005	down	(d)	-1/3	0.003
generation	neutrino	(ν_e)	0	$<10^{-9}$	up	(u)	+2/3	0.005
Second	muon	(μ^-)	-1	0.106	strange	(s)	-1/3	0.1
generation	neutrino	(ν_μ)	0	$<10^{-9}$	charm	(c)	+2/3	1.3
Third	tau	(τ^-)	-1	1.78	bottom	(b)	-1/3	4.5
generation	neutrino	(ν_τ)	0	$<10^{-9}$	top	(t)	+2/3	174

Bosons describe the interactions between the fermions , these interactions are described by the exchange of particles, which consist of the gauge bosons : photon, $W^\pm$ and Z^0, and gluons (g, eight of them), respectively. Apart from these vector bosons, there is a special scalar boson called Higgs boson, associated with the mechanism that give mass to all fundamental particles. The force experienced by the fermions is shown in table. 1.2.

Bosons are responsible for describing the interactions between fermions through the exchange of particles. These exchange particles are known as gauge bosons and include the photon, $W^\pm$, and Z^0,Additionally, there is a scalar boson called the Higgs boson, which is associated with the mechanism that gives mass to all fundamental particles. The forces experienced by fermions can be seen in table 1.2[1].

Table 1.2 Force experienced by the fermions

				Electromagnetic	**Weak**	**Strong**
Leptons	e	μ	τ	✓	✓	
	ν_e	ν_μ	ν_τ		✓	
Quarks	u	c	t	✓	✓	✓
	d	s	b	✓	✓	✓

All of these particles are described by the Standard Model (SM), which is the best theoretical model to date for providing a successful description of experimental data. However, most of this data comes from particle colliders since these particles can only be produced and studied through collisions of high energy.

1.2   Particle Colliders

Most of the recent breakthroughs in particle physics have resulted from experiments conducted at high-energy particle accelerators. These accelerators are the most powerful microscopes for observing the tiniest inner structures of cells, genes, molecules, atoms, and their constituent particles such as protons, neutrons, electrons, neutrinos, and quarks. Moreover, they may also help discover yet unknown fundamental building blocks of the universe, such as dark matter and dark energy.

Particle Colliders produce and accelerate beams of charged particles at high speeds, close to the speed of light, using electromagnetic fields ; the high-energy collisions of these beams produce individual interactions referred to as events. These collisions produce massive particles, such as the Higgs boson or the top quark. These particles only last in the blink of an eye, and cannot be observed directly, almost immediately they transform (or decay) into lighter particles, which in turn also decay. They are measured and identified by a wide range of experiments (particle detectors), whose technologies, techniques and designs are based on the properties of the particles and on the nature of their interactions with matter.

In general, a particle detector is composed of a cylindrical or polygonal barrel section, with its axis aligned parallel to the incoming colliding beams. The cylindrical structure is sealed by two flat end caps, providing almost complete solid angle coverage down to the beam pipe. The innermost region of the detector is designed for the tracking of charged particles, while the tracking volume is surrounded by an electromagnetic calorimeter that detects isolated energy deposits from electrons and photons and charged-particle tracks, respectively. The relatively large-volume hadronic calorimeter, which detects and measures the energies of hadrons, is located outside the electromagnetic calorimeter. Dedicated detectors are positioned outside the experiment to record signals from any high-energy muons produced in the collisions, which are the only particles, apart from neutrinos, that can penetrate through the hadronic calorimeter. Muons can be identified as charged-particle tracks associated with small energy depositions in both the calorimeters and signals in the muon detectors on the outside of the detector system. While neutrinos do not leave

signals in the detector, their presence can often be inferred from the presence of missing momentum.

The performance of particle colliders is typically evaluated based on two parameters: the beam energy and the luminosity. The available energy for producing new effects is one of the most important parameters, as it determines the types of particles that can be studied or discovered. Colliding beams experiments are required to achieve the necessary high center-of-mass energy. In these experiments, particles are accelerated and two beams are brought together at an intersection point where they collide. The total energy of a projectile particle and a target particle depends on the reference frame.

Colliding beam machines have the advantage that they can achieve much higher centre-of-mass energies, at various points the beams intersect and scattering takes place. If the (equal mass) incident particles have the same energy and therefore equal but opposite momentum, then the experiment is taking place in the centre-of-mass (CM) frame and the full energy delivered by the accelerator, can be used to produce high mass particles.

Consider the Lorentz invariant quantity s used in particle physics to denote the square of the total incoming energy in the CM frame:

$$s = \left(\sum_{i=1,2} E_i \right)^2 - \left(\sum_{i=1,2} p_i \right)^2 c^2 \qquad (1.1)$$

Where E and p are the energy and the momenta of each incoming particle respectively, in this frame, where the momenta are equal and opposite, the second term vanishes and:

$$s = 4E^2 \qquad (1.2)$$

The second important parameter of the collider's performance is the luminosity, defined as the quantity that measures the ability of a particle accelerator to produce the required number of interactions and is the proportionality factor between the number of events per second dR/dt and the quantum mechanical probability for the interaction called cross section σ_p.

1.3   Cross section

The technical meaning of "cross section" in particle physics is quite different from its common usage. While "cross section" typically refers to a slice of an object, in particle physics, it often refers to the probability that two particles will collide and react in a specific manner. When proton beams cross in a particle accelerator, a variety of different processes can occur. The cross section of a given process depends on the type and energy of the colliding particles. At the Large Hadron Collider (LHC), certain particles such as W and Z bosons have large cross sections σ_p, making their observation more frequent, while the production of a Higgs boson has a much lower cross section σ_p, making it more difficult to produce.

In the simplest scenario, a beam of particles of type a, with a flux denoted by ϕ_a, passes through a region of space containing n_b particles per unit volume of type b. The interaction rate per target particle r_b is proportional to the incident particle flux and can be expressed as follows [1]:

$$r_b = \sigma \phi_a$$

The essence of fundamental physics is encapsulated in σ, which has units of area and is referred to as the interaction cross section. It can be useful to conceptualize σ as the effective cross-sectional area associated with each target particle. In certain scenarios, the cross section is closely tied to the physical cross-sectional area of the target. For instance, this is the case with neutron absorption by a nucleus. Nevertheless, in general, the cross section merely represents the underlying quantum mechanical likelihood that an interaction will occur [1].

The definition of the cross section is illustrated in Figure 1.1(a) ,where a single incident particle of type a is travelling with a velocity v_a in a region defined by the area A, wish contains n_b particles of type b per unit volume moving with a velocity v_b in the opposite direction to v_a. In time δt, the particle a crosses a region containing $\delta N = nb(v_a + v_b)A\delta t$ of type b. The interaction probability can be obtained from the *effective* total cross sectional area of the δN particles divided by the area A, which can be thougth of as the probability that the incident particle passes through one of the regions of area σ drawn around each of the δN target particles, as shown in Fig. 1.1(b) [1]. The interaction probability δP is therefore

$$\delta P = \frac{\delta N \sigma}{A} = \frac{n_b(v_a + v_b)A\sigma t}{A} = n_b v \sigma \delta t, \tag{1.3}$$
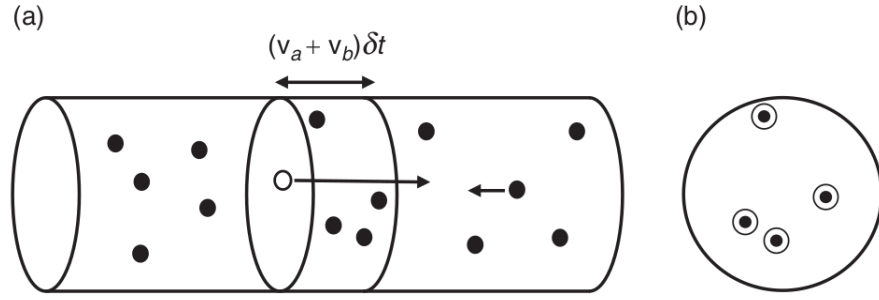
Fig. 1.1 Left hand (a): single incident particle of type a traversing a region containing particles of type b. Right-hand plot (b): projected view of the region traversed by the incident particle in time δt [1].

where $v = v_a + v_b$. The interaction rate for each particle of type a is

$$r_a = \frac{dP}{dt} = n_b v \sigma \tag{1.4}$$

For a beam of particles of type a with number density n_a confined to a volume V, the total interaction rate is

$$\text{rate} = r_a n_a V = (n_b v \sigma) n_a V = (n_a v)(n_b V) \sigma$$

$$\text{rate} = (n_a v)(n_b V) \sigma = \phi N_b \sigma$$

Thus the total rate is equal to

$$\text{rate} = \text{flux} \times \text{number of target particles} \times \text{cross section} \tag{1.5}$$

More formally, the cross section for a process is defined as

$$\sigma = \frac{\text{number of interaction per unit time per target particle}}{\text{incident flux}} \tag{1.6}$$

Where the flux ϕ accounts for the relative motion of particles. One approach to calculate the cross section for a particular process can be using the relativistic formulation of Fermi's golden rule and the appropriate Lorentz-invariant expression for the particle flux.

The cross section for the production of a general final state O at the LHC is given by [3]:

$$\sigma(pp \rightarrow O + X) = \int dx_1 dx_2 \sum_{i,j} f_i(x_1, Q) f_j(x_2, Q) \hat{\sigma}(ij \rightarrow O)(M_O, g_{ijO}, \cdots) \qquad (1.7)$$

where $f_i(x, Q)$ is the density fo partons[1] (PDF) of type i (quarks of different flavours or gluons) inside the proton, carrying a fraction x of the proton momentum at a resolution scale Q. Theory predicts the PDFs to be independent of O. $\hat{\sigma}(ij \rightarrow O)$ is the partonic cross section to produce the final state O in the collisions of partons i and j. It depends on properties of the final state (for example the mass of O, M_O, the momentum of the various particles involved, etc.), and on the the nature of the interactions involved in the process (for example the strength, g_{ijO}, of the coupling between i, j and O). Parameters like M_O and g_{ijO} are therefore what defines the underlying theory, and extracting their value as accurately as possible is the ultimate goal of an experimental measurement [3].

1.4   Luminosity

In particle physics experiments the energy available for the production of new effects is the most important parameter. Besides the energy the number of useful interactions (events), is important. The quantity that measures the ability of a particle accelerator to produce the required number of interactions is called the luminosity $\mathscr{L}_{inst}$ and is the proportionality factor between the number of events per second dR/dt and the cross section σ_p[4]:

$$\frac{dR}{dt} = \mathscr{L}_{inst} \cdot \sigma_p \qquad (1.8)$$

The unit of luminosity is $cm^{-2}s^{-1}$.

To derive a general expression for luminosity in the case of two colliding beams, we consider both beams to serve as the target and the incoming beam simultaneously. We will assume that the beams are bunched, meaning that the particles are grouped into packets or bunches.

---

[1]Before quarks and gluons were generally accepted, Feynman proposed that the proton was made up of point-like constituents, termed partons [1].
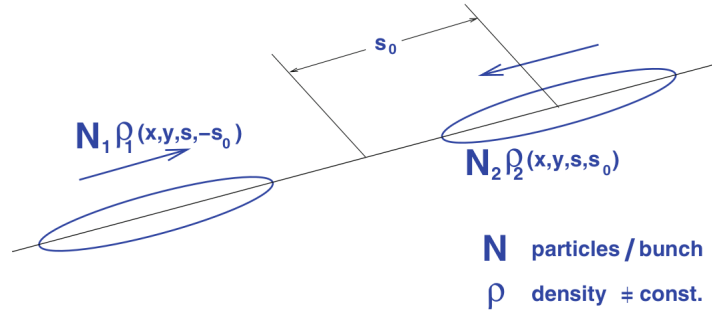
Fig. 1.2 Schematic view of a colliding beam interaction[1].

A schematic picture is shown in Fig. 1.2. Since the two beams are not stationary but are moving through each other, the overlap integral depends on the longitudinal position of the bunches, and therefore on time. As the beams move towards and through each other, the two beams have different distribution functions and a different number of particles in the beams. The overlap integral, which is proportional to the luminosity ($\mathscr{L}_{inst}$), can then be written as:

$$\mathscr{L}_{inst} \propto K \cdot \int \int \int_{-\infty}^{\infty} \rho_1(x,y,s,-s_0)\rho_2(x,y,s,s_0)dxdydsds_0 \tag{1.9}$$

Where $\rho_1(x,y,s,-s_0)$ and $\rho_2(x,y,s,s_0)$ are the time dependent beam density distribution functions. We assume, that the two bunches meet at $s_0 = 0$. Because the beams are moving against each other, we have to multiply this expression with a kinematic factor:

$$K = \sqrt{(\vec{v_1} - \vec{v_2})^2 - (\vec{v_1} \times \vec{v_2})^2/c^2} \tag{1.10}$$

Assuming head-on collisions ($\vec{v_1} = -\vec{v_2}$) and that all densities are uncorrelated in all planes. In that case we can factorize the density distributions and get for the overlap integral:

$$\mathscr{L}_{inst} = 2N_bN_1N_2f \int \int \int \int_{-\infty}^{\infty} \rho_{1x}(x)\rho_{1y}(y)\rho_{1s}(s-s_0)\rho_{2x}(x)\rho_{2y}(y)\rho_{2s}(s+s_0)dxdydsds_0 \tag{1.11}$$

where N_1 *and* N_2 are the particles per bunch, f the revolution frequency and N_b is the number of bunches in one beam.

Assuming Gaussian profiles in all dimensions of the form:

$$\rho_{iz}(z) = \frac{1}{\sqrt{2\pi}\sigma_z} exp\left(-\frac{z^2}{2\sigma_z^2}\right) \quad z = x, y \quad i = 1, 2 \tag{1.12}$$

$$\rho_s(s \pm s_0) = \frac{1}{\sqrt{2\pi}\sigma_s} exp\left(-\frac{(s \pm s_0)^2}{2\sigma_s^2}\right) \tag{1.13}$$

In the case of exactly head-on collisions of bunches travelling almost at the speed of light, the kinematic factor becomes 2, assuming approximately equal bunch lengths $\sigma_{1s} \approx \sigma_{2s}$. Solving eq. 1.11:

For a general case where $\sigma_{1x} \neq \sigma_{2x}$ and $\sigma_{1y} \neq \sigma_{2y}$:

$$\mathscr{L}_{inst} = \frac{N_1 N_2 N_b f}{2\pi\sqrt{\sigma_{1x}^2 + \sigma_{2x}^2}\sqrt{\sigma_{2y}^2 + \sigma_{2y}^2}} \tag{1.14}$$

For a specific case, asuming equal beams, $\sigma_{1x} = \sigma_{2x}, \sigma_{1y} = \sigma_{2y}$ and $\sigma_{1s} = \sigma_{2s}$:

$$\mathscr{L}_{inst} = \frac{N_1 N_2 N_b f}{4\pi\sigma_x\sigma_y} \tag{1.15}$$

This is the well known expression for the luminosity of two Gaussian beams colliding head-on. It shows how the luminosity depends on the number of particles per bunch and the beam sizes. This reflects the 2-dimensional target charge density we have seen in the evaluation of the fixed target luminosity.

In practice, the integral in 1.11 cannot be solved analytically because the properties of the colliding beams are not know precisely, so a experimental technique is implemented with a dedicated machine setup to estimate the integrals, yielding a similar expression as 1.15.

The instantaneous luminosity and therefore the maximum luminosity measure is very important because reflects the performance of the collider, but this is not the only measurement concerned with luminosity. Another important measurement and in the final figure of merit of luminosity is the so-called integrated luminosity [4]:

$$\mathscr{L}_{int} = \int_0^T \mathscr{L}_{inst}(t')dt' \tag{1.16}$$

because it directly relates to the number of observed events:

$$\mathscr{L}_{int}\sigma_p = \text{number of events of interest} \tag{1.17}$$

The integral is taken over a period of time T (excluding possible dead time). The integrated luminosity has units of cm^{-2} and is often expressed in inverse barn ($1\,barn = 10^{-24}cm^2$).

Another important parameter for a high luminosity and bunched beams is the number of collisions per bunch crossing, known as pile up (μ). The pile up and luminosity are related by the equation $f\mu = \mathscr{L}_{inst}\sigma_p$. In the case of collisions with a large cross section, this can become problematic. For the LHC, the challenge is to maximize the useful luminosity while maintaining the pile up at a manageable level for the particle detectors to handle. [4]

1.5   Importance of Luminosity precision

Understanding luminosity with the best possible precision is crucial for physics analyses such as searches for new particles, rare processes, or measurements of known particle properties. Luminosity is one of the fundamental parameters used to measure the performance of an accelerator. When two bunches of protons pass through each other, only a few protons from each bunch interact with those circulating in the opposite direction, and luminosity is a measure of the number of these interactions.

Knowing the integrated luminosity enables physicists to compare their observations with theoretical predictions and simulations. For instance, they can search for dark matter particles that escape collisions undetected by examining the energies and momenta of all particles generated in a collision. If there is an imbalance, it could be due to an undetected, potentially dark matter, particle that carries energy away. This is a powerful method of searching for new phenomena, but many effects, such as neutrinos produced in collisions, need to be considered. Neutrinos also escape undetected and leave an energy imbalance, making them indistinguishable from new phenomena. Therefore, to determine if something unexpected has been produced, physicists must look at the numbers.

If 11,000 events show an energy imbalance, and the simulations predict 10,000 events containing neutrinos, this could be significant. But if physicists only know the luminosity with a precision of 10

There are also types of analyses that depend much less on absolute knowledge of the number of collisions. For example, in measurements of ratios of different particle decays, such as the recent LHCb measurement, uncertainties in luminosity get canceled out in the ratio calculations. Other searches for new particles look for peaks in mass distribution and rely more on the shape of the observed distribution and less on the absolute number of events. But these also need to know the luminosity for any interpretation of the results.

The experimental techniques to determine signal rates are mature enough, where the understanding of acceptances, detector biases, reconstruction efficiencies, or background subtraction is at the sub-percent level, so that the final precision of the physics measurement is dominated by the luminosity uncertainty [5].

Ultimately, the greater the precision of the luminosity measurement, the more physicists can understand their observations and delve into hidden corners beyond our current knowledge.

1.6   The Large Hadron Collider

The Large Hadron Collider (LHC) is the world's largest and most powerful particle accelerator. It first started up on 10 September 2008, and remains the latest addition to CERN's accelerator complex. The LHC consists of a 27-kilometre ring of superconducting magnets with a number of accelerating structures to boost the energy of the particles along the way.

Inside the accelerator, two high-energy particle beams travel at close to the speed of light before they are made to collide. The beams travel in opposite directions in separate beam pipes – two tubes kept at ultrahigh vacuum. They are guided around the accelerator ring by a strong magnetic field maintained by superconducting electromagnets. The electromagnets are built from coils of special electric cable that operates in a superconducting state, efficiently conducting electricity without resistance or loss of energy. This requires chilling the magnets to -271.3°C – a temperature colder than outer space.

Magnets of different varieties and sizes are used to direct the beams around the accelerator. These include 1232 dipole magnets, 15 metres in length, which bend the beams, and 392 quadrupole magnets, each 5–7 metres long, which focus the beams. Just prior to collision, another type of magnet is used to "squeeze" the particles closer together to increase the chances of collisions.

The proton beams used in the LHC are produced through a series of pre-accelerators. Initially, hydrogen is ionized to produce protons, which are then accelerated in bunches up to 50 MeV in the Linear Accelerator 2 (LINAC2). Subsequently, the proton bunches

are passed through three circular accelerators: the Booster, the Proton Synchrotron (PS), and the Super Proton Synchrotron (SPS), which increase their energies to 1.4 GeV, 26 GeV, and 450 GeV, respectively. After these pre-accelerators, the proton bunches circulate in opposite directions within the LHC ring, where they are further accelerated to reach energies of up to 7 TeV per bunch. This entire process defines a single LHC fill, which typically consists of 10^{14} protons grouped into bunches to form the proton beam.

The CERN Control Centre is responsible for all the controls, services, and technical infrastructure of the LHC. From here, the proton beams are made to collide at four different locations around the accelerator ring, corresponding to the positions of the four particle detectors: Compact Muon Solenoid (CMS) [6], A Toroidal LHC Apparatus (ATLAS) [7], A Large Ion Collider Experiment (ALICE) [8], and LHCb [9]. CMS and ATLAS are general-purpose detectors designed to investigate a wide range of Standard Model (SM) and Beyond SM (BSM) physics. On the other hand, ALICE and LHCb have specialized detectors that enable them to study specific phenomena.
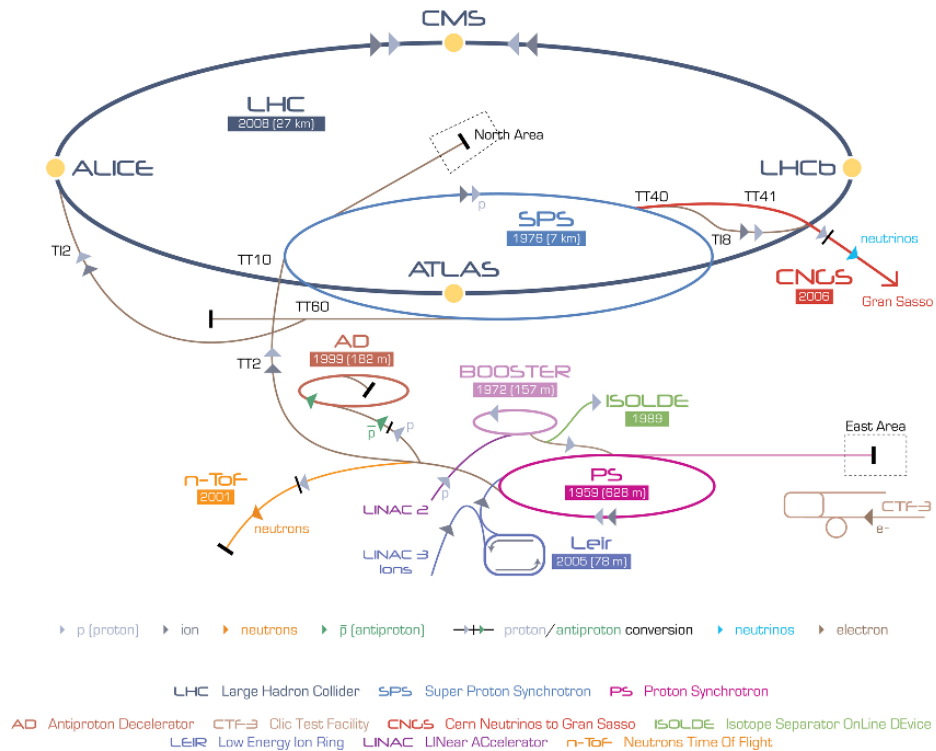

Fig. 1.3 Diagram of the LCH complex [10].

1.7   LHC Luminosity

Run 1 of the physics program at the Large Hadron Collider began in 2010 with proton-proton collisions at a center-of-mass (CM) energy of 7 TeV. By the end of 2011, CMS had collected a data sample with an integrated luminosity of $6 fb^{-1}$. This run concluded in August 2012 at a CM energy of 8 TeV, with instantaneous peak luminosities approaching 0.77×10^{34} and an integrated luminosity of $25 fb^{-1}$ [11].

Run 2 was divided into two stages. The first stage took place from 2015 to 2016, with proton-proton collisions at a center-of-mass energy of $\sqrt{s} = 13$ TeV in the CMS detector, reaching integrated luminosities of 2.2 and 36.3 fb^{-1} with relative precision of 1.6

Run 3 began in 2022 and is currently ongoing. The primary objective of this thesis project is to contribute to the improvement of the LHC luminosity precision calibration for this stage.
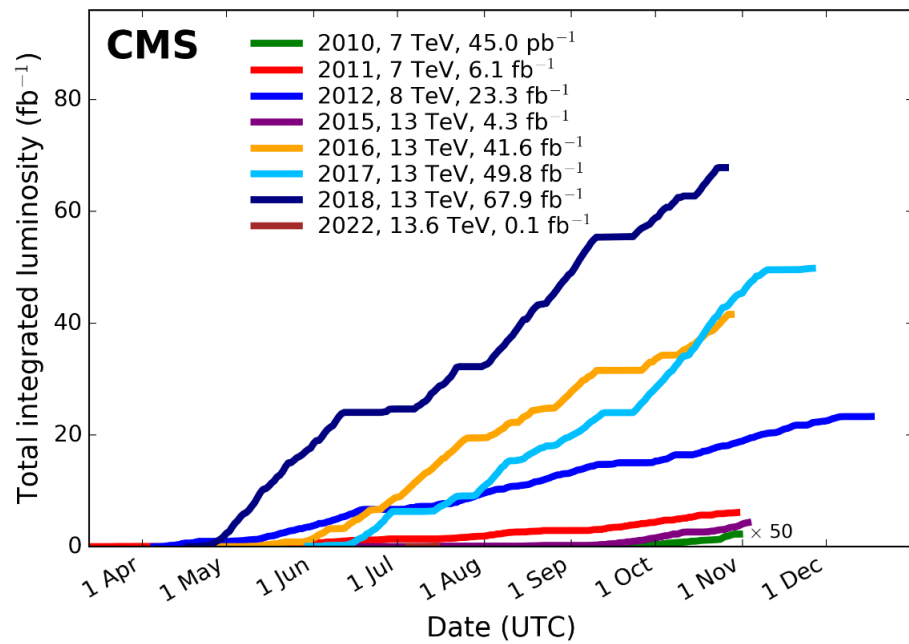

Fig. 1.4 Delivered luminosity versus time for Run-1 (2010-2012) and Run-2 (2015-2018); pp data only. Cumulative luminosity versus day delivered to CMS during stable beams for pp collisions at nominal center-of-mass energy. These plots use the best available offline calibrations for each year. For 2017 and 2018 the plots are based on [12] and [13], respectively [14].

Chapter 2

Experiment Description

Modern general-purpose detectors used in high-energy colliders typically employ cylindrical detection layers arranged around the beam axis. One such example is the Compact Muon Solenoid (CMS), which is part of the Large Hadron Collider (LHC) at CERN and is considered one of the largest international scientific collaborations in history. The CMS detector is 15 meters tall and 21 meters long, and is designed for a broad physics program that includes studying the Standard Model. This chapter provides a description of the various components of the CMS detector, with a particular focus on the silicon pixel tracker, which is described in greater detail due to its relevance to the thesis.

2.1   The Compact Muon Solenoid

The Compact Muon Solenoid (CMS) experiment is one of the four general-purpose detectors situated at the Large Hadron Collider (LHC). The CMS detector is constructed around a massive solenoid magnet, which is a cylindrical coil of superconducting cable generating a field of 4 tesla, this field is used to separate the calorimeter energy deposits of charged and neutral particles in jets. The field is confined by a steel "yoke" which constitutes the bulk of the detector's weight of 14,000 tonnes.

The CMS detector has a complete length of 21.6 meters and a diameter of 14.6 meters that comprises various detection layers that include separate parts of the detector. These layers are the fine-grained silicon tracker, which provides efficient and precise reconstruction of charged-particle trajectory. The highly-segmented electromagnetic calorimeter (ECAL) can separate energy deposits from particles in jets with high resolution. The hadronic calorimeter (HCAL) has a coarse segmentation, but it is still sufficient to distinguish between charged and neutral hadron energy deposits in jets. Additionally, there is an excellent muon tracking system, which delivers efficient and pure muon identification

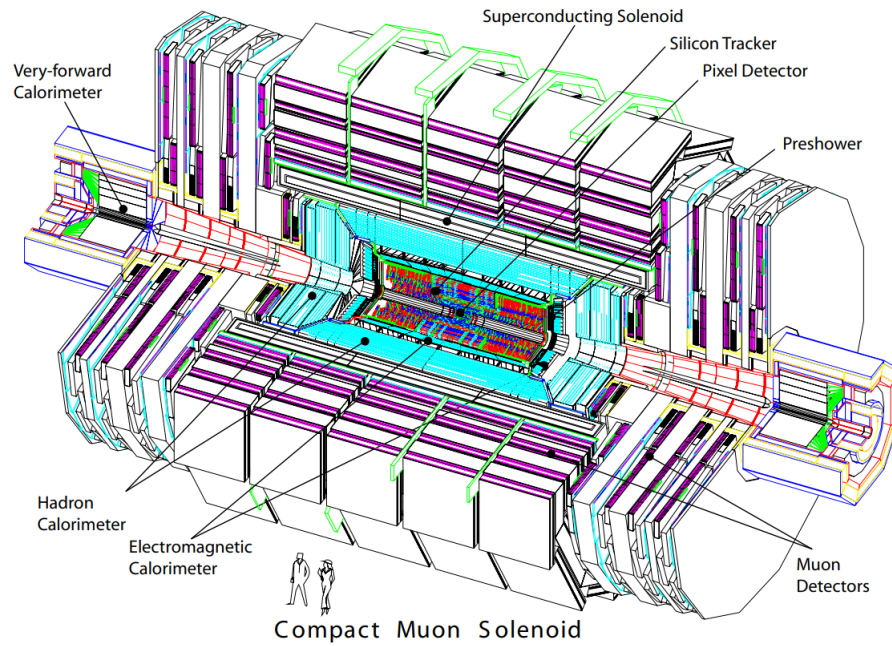regardless of the surrounding particles. A schematic representation of the CMS detector is shown in 2.1.

Fig. 2.1 Perspective view of the CMS detector.

A powerful magnet is required to bend charged particles as they travel outward from the collision point. Bending the trajectory of the particles serves two purposes: first, it helps identify the charge of the particle, as positively and negatively charged particles bend in opposite directions in the same magnetic field; and second, it enables measurement of the particle's momentum.

The CMS must identify the paths of these deflected charged particles with high precision. This is achieved using a silicon tracker composed of approximately 75 million individual electronic sensors arranged in concentric layers. When a charged particle passes through a Tracker layer, it interacts electromagnetically with the silicon and produces a hit. These individual hits can be combined to identify the track of the traversing particle.

The energies of the particles are crucial to understanding what occurred at the collision point. This information is collected from two calorimeters in the CMS. The inner layer is the Electromagnetic Calorimeter (ECAL), which measures the energy of electrons and photons by completely stopping them. It is a hermetic, homogeneous calorimeter consisting of 61,200 lead tungstate (PbWO4) crystals mounted in the central barrel part and closed by 7,324 crystals in each of the two endcaps. In front of the endcap crystals, a preshower detector is placed. Avalanche photodiodes (APDs) are used as photodetectors in

the barrel and vacuum phototriodes (VPTs) in the endcaps. Hadrons, which are composite particles made up of quarks and gluons, travel through the ECAL and are stopped by the outer layer, called the Hadron Calorimeter (HCAL).

The final particle that the CMS directly observes is the muon. Muons are approximately 200 times heavier than electrons and are not stopped by the calorimeters. Therefore, special sub-detectors have to be constructed to detect them as they traverse the CMS. These sub-detectors are interleaved with the return yoke of the solenoid. The large magnet of the CMS also allows us to measure each muon's momentum both inside the superconducting coil (using the tracking devices) and outside of it (using the muon chambers). A transverse slice of the CMS detector, depicting specific particle interactions, is shown in Figure 2.2.
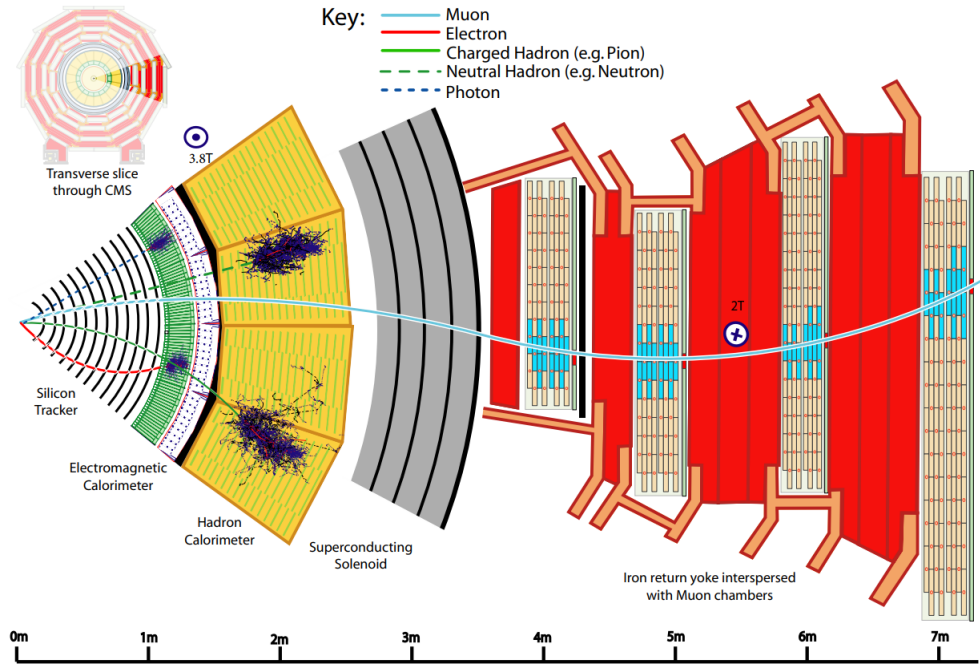
Fig. 2.2 Sketch of a transverse slice of the CMS detector with specific particle interactions, from the beam interaction region to the muon detector. The muon and the charged pion are positively charged, and the electron is negatively charged [15].

The coordinate system adopted by CMS has the origin at the center of the detector, the y-axis pointing vertically upward, and the x-axis pointing radially inward toward the center of the LHC. Thus, the z-axis points along the beam direction toward the Jura mountains from LHC Point 5. The azimuthal angle φ is measured from the x-axis in the $x-y$ plane and the radial coordinate in this plane is denoted by r. The polar angle θ is measured from the z-axis. Pseudorapidity is defined as $\eta = -\ln\tan(\theta/2)$ [6].

2.2 CMS Tracking System

The tracking system plays a crucial role in precisely measuring the trajectories and momenta of charged particles generated by collisions in the LHC, as well as reconstructing secondary vertices. It has a physical size of 5.8 m in length and 2.5 m in diameter and is surrounded by the CMS solenoid, which provides a homogeneous magnetic field of 4 T throughout the tracker's volume.

The CMS tracker consists of two parts: a pixel detector with three barrel layers located between 4.4 cm and 10.2 cm radii and a silicon strip tracker with ten barrel detection layers extending to a radius of 1.1 m. Each part includes endcaps, with the pixel detector having two disks and the strip tracker having three plus nine disks on each side of the barrel. This extends the tracker's acceptance up to a pseudorapidity of $|\eta| < 2.5$, with an active silicon area of approximately 200 m^2. The construction of the CMS tracker required the development of new production methods and quality control procedures in order to produce its 1440 pixel and 15148 strip detector modules. The layout of the CMS tracker is presented in the following figure:
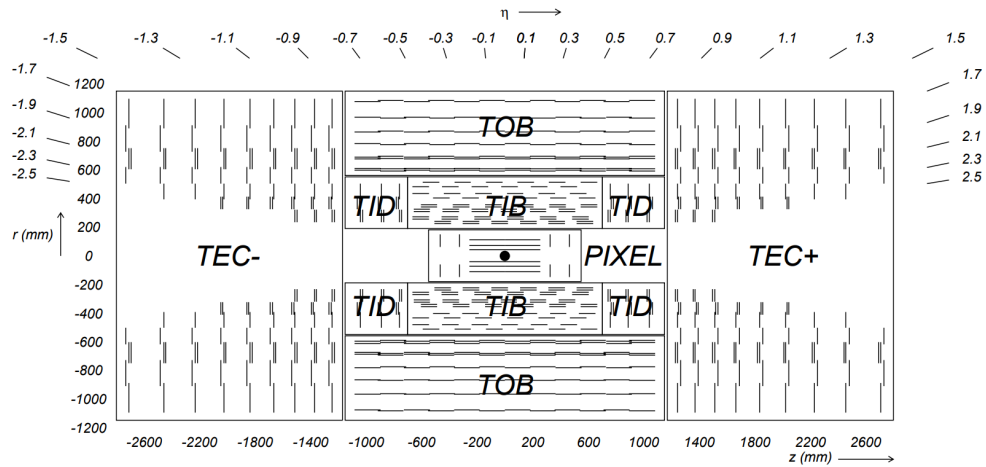
Fig. 2.3 Schematic cross section through the CMS tracker. Each line represents a detector module [6]. The Pixel tracker here is not the CMS Phase-1 pixel detector.

As a charged particle traverses a medium, it creates a trail of ionized atoms and liberated electrons. By detecting this ionization, it is possible to reconstruct the trajectory of the charged particle. In each cylindrical layer of a silicon sensor, a charged particle will leave a hit, which enables the reconstruction of the charged particle track [1].

The interaction of a charged particle with a medium results in electromagnetic interaction with the atomic electrons, leading to energy loss through atomic ionization [1]. The

theory governing such losses is predominantly due to Coulomb scattering from the atomic electrons, which was established by Bethe, Bloch, and others in the 1930s. The resulting formula, known as the Bethe-Bloch formula, is expressed as [16]:

$$-\frac{dE}{dx} = \frac{Dq^2 n_e}{\beta^2}\left[\ln\left(\frac{2m_e c^2 \gamma^2}{I}\right) - \beta^2 - \frac{\delta(\gamma)}{2}\right] \qquad (2.1)$$

x is the distance travelled through the medium, m_e is the electron mass, $\beta = v/c$, $\gamma = (1 - \beta^2)^{-1/2}$ and $D = \frac{4\pi\alpha^2\hbar^2}{m_e} = 5.1\times10^{-25}\text{MeV cm}^2$. The other constants refers to the medium: n_e is the electron density, I is the mean ionisation potencial of the atoms averaged over all electrons (given approximately by I=10ZeV for $Z >$20) and δ is a dielectric screening correction that is only important for highly relativistic particles.

The CMS tracking detector relies on semiconductor technology that uses silicon pixels and strips. This tracking system is made up of two subsystems: the pixel tracker, which is the closest to the interaction point, and the strip tracker [6]. The following section will provide a description of the pixel detector.

2.2.1   Pixel Detector and Clustering

The CMS experiment conducted at the Large Hadron Collider (LHC) at CERN comprises a silicon pixel detector, which forms the innermost component of the tracking system. This detector facilitates the provision of 3-dimensional space points in the area nearest to the interaction point, which, in turn, enables precise tracking of charged particles and vertex reconstruction. The pixel detector operates in a radiation-rich environment, marked by high track density.

The CMS pixel detector encompasses four concentric barrel layers (L1-L4), each with radii measuring 29, 68, 109, and 160 mm, and three disks (D1-D3) on either end positioned at distances of 291, 396, and 516 mm from the detector's center. A schematic of the CMS Phase-1 pixel detector's arrangement is depicted in Figure 2.4 where the total silicon area of the CMS Phase-1 pixel detector spans 1.9 square meters. The pixel detector comprises 1856 segmented silicon sensor modules, with 1184 modules used in the barrel pixel detector (BPIX) and 672 modules in the forward disks (FPIX). Each module features a sensor with 160 by 416 pixels, connected to 16 readout chips (ROCs), resulting in 124 million readout channels in total.

The BPIX and FPIX detectors are equipped with four service half-cylinders each, with a combined length of 540 mm. These cylinders host the readout and control circuits,
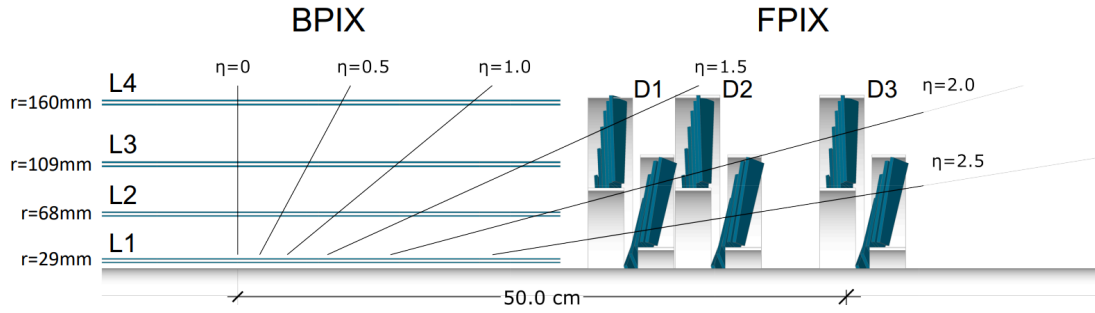
Fig. 2.4 Layout of the CMS Phase-1 pixel detector in longitudinal view[17].

and provide guidance for the power lines and cooling tubes of the detector. The BPIX detector is bifurcated into two mechanically self-sufficient halves, both of which are made up of a half detector and two service half-cylinders. The orientation of the sensor surface of the modules in both halves is parallel to the magnetic field. On the other hand, the FPIX detector is segmented into four mechanically independent quadrants, each of which comprises three half-disks housed in a service half-cylinder. The sensor orientation in the FPIX detector is arranged such that the long side of the pixel is aligned with the radial direction and has a coverage from 45 to 161 mm. The half-disks are additionally subdivided into inner and outer half-rings that support 22 and 34 modules, respectively.

The CMS Phase-1 pixel detector is built from 1856 segmented silicon sensor modules, where 1184 modules are used in the barrel pixel detector (BPIX) and 672 modules are used for the forward disks (FPIX). Each module consists of a sensor with 160×416 pixels connected to 16 readout chips (ROCs). In total there are 124 million readout channels [17]. A pixel detector module is built from a planar silicon sensor with a size of 18.6×66.6 mm^2 (active area of 16.2×64.8 mm^2), bump-bonded to an array of 2×8 ROCs. Each ROC is segmented into 4160 readout channels and reads out the pulse height information for each pixel. The standard pixel size is 100×150 μm^2, as in the original pixel detector. The figures depicting the modules of the CMS Phase-1 pixel detector can be found in Figure 2.5 [17].
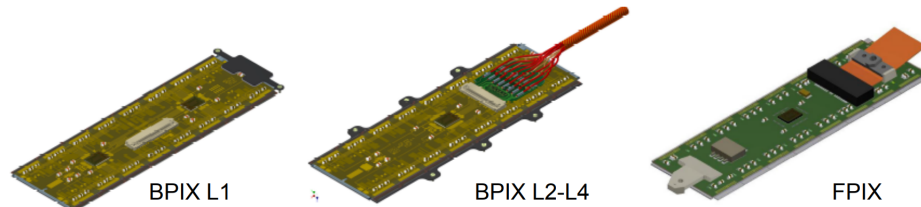

Fig. 2.5 Drawings of the pixel detector modules for BPIX L1 (left), BPIX L2–4 (middle), and the FPIX detector (right)[17].

The track reconstruction process involves several steps. Firstly, zero-suppressed signals above specified thresholds in pixel channels are clustered into hits. These hit pixels are then combined to form clusters from neighboring pixels. The charge measured within each cluster corresponds to the charge deposited by a single charged particle. Next, the cluster positions and their uncertainties are estimated in a local orthogonal coordinate system (u, v) in the plane of each sensor.

The pixel sensor used in this process consists of $100 \times 150 \mu m^2$ pixels with the u-axis oriented parallel to the shorter pixel edge, this is shown en the figure 2.6. To be considered a valid cluster, each one must have a minimum charge equivalent to 4000 electrons [18, 17]. For normally incident minimum-ionizing particles (MIPs) in a silicon sensor with a thickness of 285 μm, the most probable value of energy deposition corresponds to approximately 21000 electrons. However, this charge is often spread over more than one pixel due to Lorentz drift and diffusion of collected electrons, leading to charge clusters.
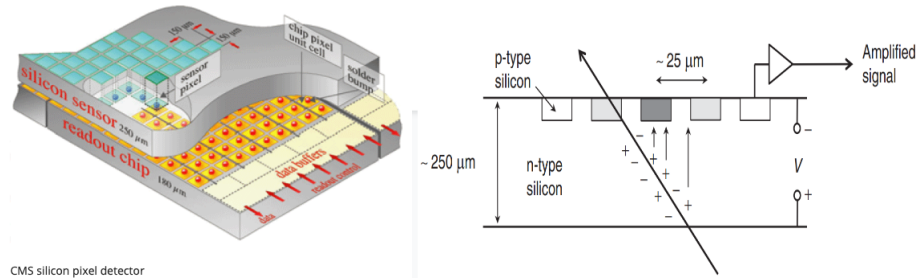

Fig. 2.6 left: Pixel sensor diagram, right: hits detection in pixel sensor.

2.2.2 CMS Luminometers

A total of seven systems are used for measuring luminosity at CMS. The Pixel Luminosity Telescope (PLT) and Fast Beam Conditions Monitor (BCM1F) are dedicated systems for luminosity measurement, while the hadronic forward calorimeter (HF) uses a dedicated readout on an existing system. Additionally, three other methods, the drift tube luminosity (DT), the pixel cluster counting method (PCC), and the vertex counting method (VTX), use data from existing parts of the CMS detector to perform a luminosity measurement using the main CMS DAQ system. The PCC measurement uses the data collected with the standard CMS trigger system with triggers requiring colliding bunches but not any specific event activity, known as "zero-bias" triggers. Finally, the RAMSES detectors are part of

the LHC environmental protection and monitoring systems, but they can also be used to provide a luminosity measurement readout through Timber, the operational data and LHC logging service [13].

The PLT is a dedicated system for measuring luminosity using silicon pixel sensors. There are a total of 48 sensors arranged into 16 "telescopes",the rate of "triple coincidences," where a hit is observed in all three planes, is measured.

BCM1F comprises a total of 24 sensors mounted on the same carriage as the PLT, consisting of 10 silicon sensors, 10 polycrystalline diamond (pCVD) sensors, and 4 single-crystal diamond (sCVD) sensors.

The HF luminosity measurement uses a dedicated readout system installed in the HF calorimeter. Only two HF rings are used for luminosity measurement to ensure relatively uniform occupancy. Two algorithms are available: the first relies on the fraction of occupied towers (HFOC), and the second is based on the sum of the transverse energy ET (HFET).

Drift tube luminosity (DT), which uses the rate of muon track stubs in the muon barrel track finder and RAMSES detectors, a CERN radiation and environmental monitoring system, although not designed as a luminometer, function quite well as a luminosity measurement, using the rate observed in the detectors (primarily photons within the energy range of 50 keV to 7 MeV). Another method is the pixel cluster counting (PCC), which will be described in more detail in chapter 3 [13].

Chapter 3

Luminosity Measurement and Calibration

Accurately measuring the luminosity delivered to the CMS experiment by the LHC is essential for various reasons. Online, the luminosity measurement provides feedback on the LHC and CMS performance and operations, including measuring trigger rates. In offline analysis, the luminosity measurement is a critical component for measuring the cross-section of observed processes or setting upper limits in searches for processes beyond the standard model.

To measure luminosity, a total of seven luminometers are used at CMS, and each of them reads out a specific quantity observed in the detector, such as hits, tracks, or clusters. The rate R measured by the luminometer is proportional to the instantaneous luminosity, $\mathscr{L}_{inst}$, with the constant of proportionality given by the visible cross-section σvis [13].

$$R(t) = \mathscr{L}_{inst}\sigma_{vis} \tag{3.1}$$

The determination of σ_{vis} is carried out through van der Meer (vdM) scans performed with a dedicated LHC machine setup.

3.1 Pixel Cluster Counting method

The PCC method utilizes the rate of pixel clusters in the CMS pixel detector to determine the luminosity. The pixel detector's large area and low occupancy yield measurements with excellent linear response and high statistical precision. However, the statistical precision for a single 23-second period or "luminosity section" is not as high as for online luminometers due to the limited CMS trigger bandwidth available for collecting data. Nonetheless,

over longer time periods, this method provides a stable and highly precise luminosity measurement. On average, the detector occupancy is less than 0.1% [13].

To obtain the mean number of pixel clusters per event, several zero-bias events are averaged. This value is given by :

$$\langle N_{\text{cluster}} \rangle = \langle N_{\text{pixel/interaction}} \rangle \langle N_{\text{interactions}} \rangle \equiv \langle N_{\text{pixel/interaction}} \rangle \mu \tag{3.2}$$

where in the last step, the average number of interactions per bunch crossing, pileup, is denoted by the symbol μ [19].

In the PCC measurement, the innermost layer of the pixel detector is excluded from the analysis due to significant dynamic inefficiency effects. At higher $\mathscr{L}_{inst}$, the hit efficiency in this layer decreases because the readout chip cannot process all of the hits. Only modules that consistently perform well for luminosity purposes throughout the year are utilized in the measurement.

For the VdM measurement, a special trigger mode is employed, which enables a higher data rate for PCC to acquire the required statistical precision. However, this mode is only active for five bunch crossings, and data are taken exclusively during this period.

3.2 Luminosity calibration: van der Meer method

As we saw in chapter 1 the instantaneous luminosity for a single colliding bunch is guiven by 1.11, in practice The measurement of the beam currents Ni is well determined, but the individual proton density functions cannot be directly measured. The VdM method is a dedicated machine setup determines the value of the two beam overlap integrals obteniendo density profiles close to normal distributions by varying the beam separation and measuring the resulting rates:,

$$\int \rho_{x1}(x)\rho_{x2}(x)dx = \frac{R_x(0)}{\int R_x(\Delta)d\Delta} \tag{3.3}$$

where $R_x(\Delta)$ is the rate measured when the two beams are separated in x by a distance Δ; a asimilar equation can be written in y. Then the beam overlap width Σ_x (and similarly Σ_y) is defined as [13]:

$$\Sigma_x = \frac{1}{\sqrt{2\pi}} \frac{\int R_x(\Delta)d\Delta}{R_x(0)} \tag{3.4}$$

yielding the final expression for luminosity (for one single bunch):

$$\mathscr{L}_{inst} = \frac{N_1 N_2 f}{2\pi\Sigma_x\Sigma_y} \tag{3.5}$$

where $N_{1,2}$ are the particles per bunch (bunch current) and $f = 11246$ Hz is the bunch orbit frequency around the LHC ring.

3333 This expression can be finally used in 3.1 to get σ_{vis}:

$$\sigma_{vis} = \frac{2\pi\Sigma_x\Sigma_y R(0,0)}{N_1 N_2 f} \tag{3.6}$$

Experimentally, two separate scans in the x and y directions are performed. The beams are scanned against each other while measuring the rate (normalized by the product of the beam currents) at a certain number of separation steps, fitting the resulting points with a functional form, and using the fitted function to extract $\Sigma_{x,y}$ and $R(0,0)$ in 3.6. Fig. 3.1 shows an sketch of the beam positions during vdM scans in X and Y planes together with the detector rate as a function of beam separation.
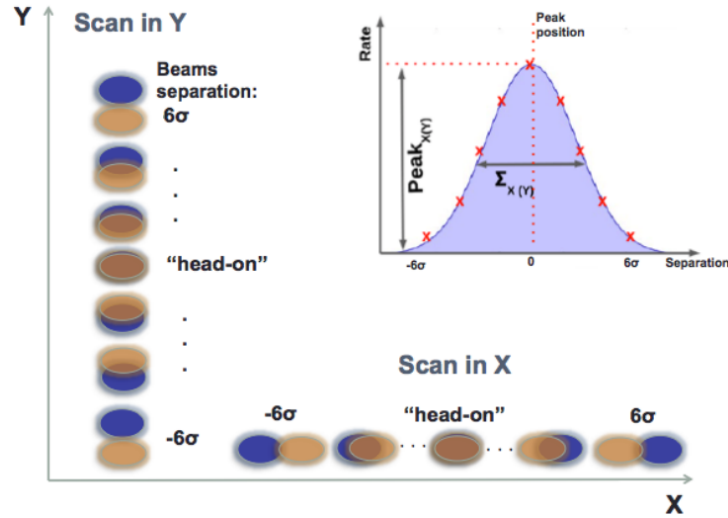

Fig. 3.1 The sketch of a vdM scan in X and Y planes. The indent sketch is an example of the fitting of the resulting rates [20].

References

[1] Mark Thomson. *Modern Particle Physics*. Cambridge University Press, 2013. doi: 10.1017/CBO9781139525367.

[2] David J Griffiths. *Introduction to elementary particles; 2nd rev. version*. Physics textbook. Wiley, New York, NY, 2008. URL https://cds.cern.ch/record/111880. https://cds.cern.ch/record/111880.

[3] M.L. Mangano, Motivations and precision targets for an accurate luminosity determination at the LHC, *CERN-Proceedings-2011-011*, https://cds.cern.ch/record/1347440.

[4] Stephen Myers and Herwig Schopper. *Particle Physics Reference Library Volume 3: Accelerators and Colliders*. 01 2020. doi: 10.1007/978-3-030-34245-6.

[5] P. Grafström and W. Kozanecki. Luminosity determination at proton colliders. *Progress in Particle and Nuclear Physics*, 81:97–148, 2015. doi: https://doi.org/10.1016/j.ppnp.2014.11.002.

[6] CMS Collaboration. The CMS experiment at the CERN LHC. *Journal of Instrumentation*, 3(08):S08004–S08004, Aug 2008. doi: 10.1088/1748-0221/3/08/s08004.

[7] ATLAS Collaboration. The ATLAS experiment at the CERN large hadron collider. *Journal of Instrumentation*, 3(08):S08003–S08003, Aug 2008. doi: 10.1088/1748-0221/3/08/s08003.

[8] ALICE Collaboration. The ALICE experiment at the CERN LHC. *Journal of Instrumentation*, 3(08):S08002–S08002, Aug 2008. doi: 10.1088/1748-0221/3/08/s08002.

[9] The LHCb Collaboration. The LHCb detector at the LHC. *Journal of Instrumentation*, 3(08):S08005–S08005, Aug 2008. doi: 10.1088/1748-0221/3/08/s08005.

[10] Eva Halkiadakis. Introduction to the LHC Experiments. In *Theoretical Advanced Study Institute in Elementary Particle Physics: Physics of the Large and the Small*, pages 489–518, 2011. doi: 10.1142/9789814327183_0009.

[11] Mike Lamont. Status of the LHC. *Journal of Physics: Conference Series*, 455: 012001, Aug 2013. doi: 10.1088/1742-6596/455/1/012001.

[12] CMS luminosity measurement for the 2017 data-taking period at $\sqrt{s} = 13$ TeV. Technical report, CERN, Geneva, 2018. URL https://cds.cern.ch/record/2621960.

[13] CMS luminosity measurement for the 2018 data-taking period at $\sqrt{s} = 13$ TeV. Technical report, CERN, Geneva, 2019. URL https://cds.cern.ch/record/2676164.

[14] CMSPublic Web. CMS Luminosity - Public Results. Delivered luminosity versus time for 2010-2012 and 2015-2018 (pp data only), 2022. URL https://twiki.cern.ch/twiki/bin/view/CMSPublic/LumiPublicResults. [Online; accessed September 23, 2022].

[15] A.M. Sirunyan et al. Particle-flow reconstruction and global event description with the CMS detector. *Journal of Instrumentation*, 12(10):P10003–P10003, Oct< 2017. doi: 10.1088/1748-0221/12/10/p10003.

[16] Brian R Martin and Graham Shaw. *Particle Physics*. Manchester Physics Series. John Wiley & Sons, Nashville, TN, 4 edition, January 2017.

[17] W. Adam et al. The CMS phase-1 pixel detector upgrade. *Journal of Instrumentation*, 16(02):P02027–P02027, Feb 2021. doi: 10.1088/1748-0221/16/02/p02027.

[18] The CMS Collaboration. Description and performance of track and primary-vertex reconstruction with the CMS tracker. *Journal of Instrumentation*, 9(10):P10009–P10009, Oct 2014. doi: 10.1088/1748-0221/9/10/p10009.

[19] CMS Luminosity Based on Pixel Cluster Counting - Summer 2012 Update. Technical report, CERN, Geneva, 2012. URL https://cds.cern.ch/record/1482193.

[20] Olena Karacheban. Performance of the BRIL luminometers at CMS in Run 2. *PoS*, EPS-HEP2019:194, 2020. doi: 10.22323/1.364.0194.